Suppression of Self-nucleation Effect of Semi-crystalline Polymers by Confinement

Ming Wang[1,2 #], Jing Li[1 #], Guangyu Shi[1], Guoming Liu*[1,2], Alejandro J. Müller[3,4] and Dujin Wang[1,2]

1. Beijing National Laboratory for Molecular Sciences, CAS Key Laboratory of Engineering Plastics, CAS Research/Education Center for Excellence in Molecular Sciences, Institute of Chemistry, Chinese Academy of Sciences, Beijing 100190, China
2. University of Chinese Academy of Sciences, Beijing 100049, China
3. POLYMAT and Department of Polymers and Advanced Materials: Physics, Chemistry and Technology, Faculty of Chemistry, University of the Basque Country UPV/EHU, Paseo Manuel de Lardizabal 3, 20018 Donostia-San Sebastián, Spain
4. IKERBASQUE, Basque Foundation for Science, Bilbao 48013, Spain

# equal contribution

* corresponding author: gmliu@iccas.ac.cn

For Table of Content use only

Suppression of Self-nucleation Effect of Semi-crystalline Polymers by Confinement

Ming Wang[1,2 #], Jing Li[1 #], Guangyu Shi[1], Guoming Liu*[1,2], Alejandro J. Müller[3,4] and Dujin Wang[1,2]

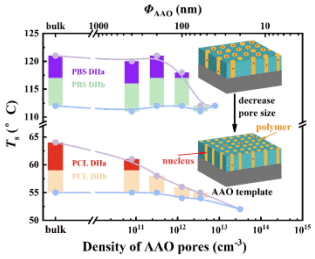

ABSTRACT

The *melt memory effect* is well-known in polymer crystallization. It is caused by self-nuclei that persist above the melting temperature. The origin and physical nature of self-nuclei are still under debate. In this work, we studied the effect of confinement on the self-nucleation behavior of two typical semicrystalline polymers: poly(ε-caprolactone) (PCL) and poly(butylene succinate) (PBS) using anodic aluminum oxide (AAO) templates. The density of AAO nanopores covers a range of $10^{11} \sim 10^{13}$ cm^{-3}. Narrowing of the self-nucleation region (*Domain II*) with a decrease of AAO diameter was observed for both infiltrated PCL and PBS, indicating the suppression of the self-nucleation effect. When the diameter of AAO is below 60 nm, *Domain II* vanished. Further analysis indicated that *Domain IIa* (*melt memory region*) vanished first, followed by *Domain IIb (self-seeding region)*. The results provide a method of estimating the self-nuclei density of different polymers at different temperatures.

1. INTRODUCTION

A unique feature of polymer crystallization is the "*melt memory effect*".[1-4] In a typical differential scanning calorimetry (DSC) experiment[2] performed to study the self-nucleation behavior, when a semi-crystalline polymer is heated to a temperature (denoted self-nucleation temperature or T_s) that is high enough to erase the "thermal history", the polymer will show an identical crystallization temperature during subsequent cooling, independent of T_s. This behavior is characteristic of "*Domain I*" where all crystalline memory is lost (also called melting Domain). If T_s is not high enough to reach the isotropic melt state, the sample will crystallize at a higher temperature during cooling with decreasing T_s. However, the melting temperature is essentially unaltered. This T_s region is called "*Domain II* or *Self-nucleation Domain*". Reducing T_s even further, the material enters "*Domain III*" or self-nucleation and annealing domain. As T_s is too low, the sample is only partially melted. Unmelted crystals will be annealed during the time that the sample stays at T_s, and a higher melting peak will be seen in the second heating, after cooling from T_s. The reason for the enhanced crystallization in *Domain II* is the existence of self-nuclei at T_s.

Domain II has been further divided into two sub-domains based on the different origins of the

self-nuclei[3, 4]: (a) *Domain IIa*, at temperatures higher than the T_m at which the melting peak completely disappears in a DSC heating trace, i.e., where all the polymer crystals are completely molten but without erasing the melt memory in the higher temperature range of *Domain II*; (b) *Domain IIb*; where some crystal fragments are left to act as *self-seeds* in the low part of *Domain II*. *Domain IIa* corresponds to the melt memory *Domain*, while *Domain IIb* is the self-seeding *Domain*. The entire *Domain II* is termed the *self-nucleation Domain*, as it encompasses all types of self-nuclei capable of enhancing nucleation density in the material (i.e., self-seeds and melt memory effects).

The self-nucleation phenomenon has been observed under conditions of solution crystallization and melt crystallization in homopolymers and copolymers.[3] In general, the nucleation density becomes larger and consequently, the spherulitic size becomes smaller in *Domain II*.[5] The typical concentration of self-nuclei under ideal T_s is in the range of 10^9-10^{12} cm^{-3}.[3] It is noted that the transition temperatures of domains are influenced by the experimental parameters including the time spent at T_s, and heating/cooling rate.[6]

The origin of self-nuclei has been interpreted as crystalline remnants[2, 7], residual orientation of chain segments[5], topological effects[8], or metastable melt states[9]. Different characterization methods have been applied to detect the structure of self-nuclei[7, 10-12]. However, no conclusive result has been obtained. Recently, rheological techniques and dielectric relaxation spectroscopy were shown to be capable of detecting the difference between the isotropic and self-nucleated melts.[13-15] It was observed, that the time-temperature superposition (TTS) failed in self-nucleated propylene-ethylene copolymers[13]. A more dramatic difference was observed in poly(ε-caprolactone) (PCL). The self-nucleated PCL exhibited higher viscosity, higher flow activation energy, higher plateau modulus, and lower electrical permittivity value as compared to the isotropic melt.[14, 15] Liu et al.[16] has observed a narrowing of *Domain II* when the density of hydrogen bonds is diluted by increasing the number of methylene in polyamide (PA). The relationship between melt memory and intermolecular interactions was further demonstrated in a series of polycarbonates, polyesters, polyethers, and polyamides.[17] In copolymers, Hu and Alamo have shown that the strong melt memory effect is attributed to the clusters of long ethylene

sequences in a "heterogeneous melt".[10, 18]

Confinement influences the melt memory effect significantly. When a polymer is divided into microdomains, the nucleation process will be confined to each microdomain. Classical self-nucleation behavior has been reported in block copolymers when the melt is miscible or weakly segregated or when the segregated crystalline phases are interconnected, such as in lamellar or cylindrical phases.[19-21] For crystallization in block copolymer with isolated microdomains (cylinders or spheres), *Domain II* vanishes possibly because the number of microdomains is much larger than that of self-nuclei generated or because of the macromolecular topological effects caused by strong confinement.[19, 22] Vanishing of *Domain II* has also been observed in poly(butylene terephthalate)/reduced graphene oxide nanocomposite[23] and methoxypolyethylene glycol (MPEG) grafted onto nanosilica.[24]

Although many interesting observations have been reported for the self-nucleation effect of polymers under confinement, the effect of domain size has not been explored yet. A disadvantage of using block copolymers as the model system is that the size of domains cannot be tuned in a broad range while maintaining the same morphology. On the other hand, the confinement size of nanocomposites is not well-defined. Anodic aluminum oxide templates (AAO), with isolated, uniform cylindrical microdomains covering a diameter range of 500 nm to 10 nm, have been used as an ideal model system to understand the crystallization under confinement.[25-28] It has been demonstrated that the crystallization of polymers changes under confinement in AAO. The results in the literature indicate that polymers undergo a transition of nucleation mechanism from heterogeneous to homogeneous or surface nucleation[29, 30], preferred crystal orientation[31-34], "nucleation-dominated" crystallization kinetics[35-38], and metastable crystalline modification and retarded polymorphic transition[39, 40].

In this work, we examine the effect of confinement on the self-nucleation *Domains* of two typical semicrystalline polymers: PCL and poly(butylene succinate) (PBS) within AAO. The reason for selecting these two polymers is the relatively broad temperature range of *Domain II,* which includes both *Domain IIa* and *Domain IIb*. The diameter of the AAO nanopores varied from 20 nm to 400 nm. For the first time, we show a continuous change of the width of the

self-nucleation *Domain* as a function of nanopore size.

2. EXPERIMENTAL SECTION

2.1. Materials and Sample Preparation.

PCL and PBS were purchased from Sigma Aldrich. The number-average molecular weight (M_n) and the polydispersity index of PCL are 10,000 g/mol and 1.4, respectively. The PBS has a weight-average molecular weight (M_w) of 15,000 g/mol. The AAO templates with pore diameters (Φ) of 400, 200, 100, 60, 40, and 20 nm were supplied by Shanghai Shangmu Technology Co. Ltd. The lengths of the AAO pores are approximately 100 μm for all the templates. The AAO templates were degassed under vacuum at 200 ºC for 2 hours before infiltration.

The infiltration of PCL and PBS was performed in a home-made vacuum chamber with a temperature controller. After cooling down to room temperature, polymer films were placed on the surface of AAO, followed by treatment at 100 ºC (for PCL) or 180 ºC (for PBS) under vacuum for 5 h and then under a nitrogen atmosphere for 5 h. According to the procedure recommended by Shi et al.,[41] the residual polymer on the surface of AAO was carefully cleaned with a sharp blade and gauze at a temperature where the polymer is in a molten state, and then further cleaned using a mixture of chloroform and ethanol (volume ratio 1:1) at room temperature.

2.2. Characterization.

A Hitachi S-4800 scanning electron microscope (SEM) was utilized to examine the AAO templates and confined polymer samples. To observe PCL and PBS nanorods within the AAO templates, the templates filled with polymer were fractured. The microscope was operated at 10 kV. Before SEM observations, the samples were coated with gold.

A heat-flux DSC (Q 200, TA) was used to examine the thermal behavior of the samples. The calorimeter was calibrated with indium before experiments. The polymer-infiltrated AAO samples with a mass of 6~10 mg were sealed in aluminum pans. All the measurements were carried out under a helium atmosphere with a flow rate of 25 mL/min. For PCL, the scanning range was between -80 °C and 90 °C. For PBS, the samples were scanned between -40 °C and 140 °C. The heating and cooling rates were 20 °C/min. The heat flow of the infiltrated samples was normalized

by the total mass of the AAO template and polymer inside it. Thus, the absolute values of the heat flow have no physical meaning.

The thermal protocol of the self-nucleation experiments using DSC is shown in Figure 1, based on Fillon et al.[2] and later references.[3, 4] This protocol consists of several steps as follows:

(1) Heat to a temperature at about 30 °C above the melting temperature of the sample for 3 min to erase the thermal history. PCL and PBS samples were heated to 90 °C and 140 °C, respectively.
(2) Cool at 20 °C/min down to a low temperature at which the non-isothermal crystallization process has finished, to obtain the standard crystallization temperature and standard crystalline state of the sample.
(3) Heat at 20 °C/min to a temperature denoted as self-nucleation temperature (T_s) and keep for 5 min.
(4) Cool from T_s to the chosen lower temperature limit at 20 °C/min.
(5) Heat at 20 °C/min to the temperature established in step (1) to erase the thermal history.
(6) Repeat steps 3-5 to get the three characteristic domains.

Three different self-nucleation domains can be defined depending on T_s: In *Domain I*, the sample is completely molten into a homogeneous melt, and the crystallization temperature is independent of T_s. *Domain II* shows higher crystallization temperature (due to the nucleating effect of self-nuclei, i.e., produced by melt memory in *Domain IIa* and produced by self-seeds in *Domain IIb*) but no effect on the melting temperature. In *Domain III*, crystals are not completely molten. Therefore, the sample will be self-seeded and the residual unmolten crystals will be annealed, showing an increased T_c and an additional melting peak corresponding to the annealed crystals.

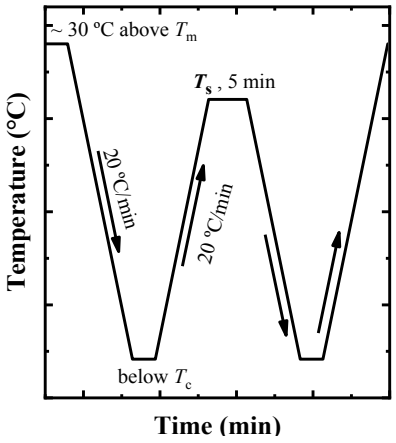

Figure 1. Thermal protocol of a self-nucleation (SN) experiment.

3. RESULTS AND DISCUSSION

3.1. Morphology of PCL and PBS within AAO Nanopores.

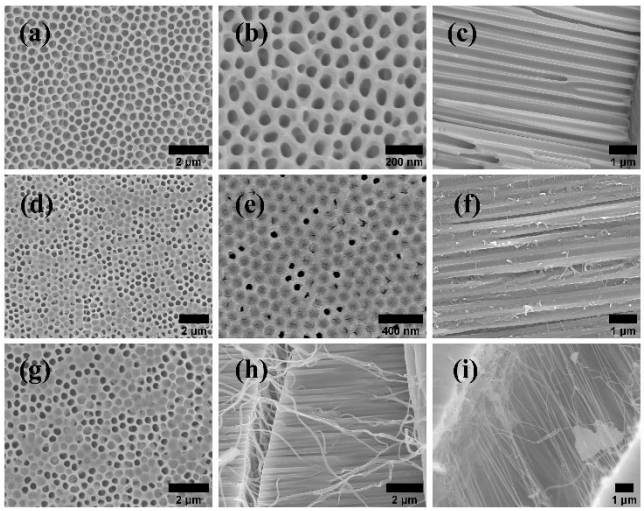

Figure 2. SEM micrographs of AAO templates and infiltrated samples: top view of empty AAO with Φ = 400 (a) and Φ = 100 nm (b); cross-sectional images of empty AAO with Φ = 400 nm (c); top view of the infiltrated PCL inside the AAO with Φ = 400 nm (d) and Φ = 100 nm (e); cross-sectional view of the infiltrated PCL inside the AAO with Φ = 400 nm (f); top view of the infiltrated PBS inside the AAO with Φ = 400 nm (g); cross-sectional view of the infiltrated PBS inside the AAO with Φ = 200 nm (h) and Φ =100 nm (i).

Figure 2 shows the SEM images of AAO templates and polymer nanorods. The appearance of

the surface of empty AAO templates with diameters of 400 nm and 100 nm respectively (Figures 2a and 2b) indicates the diameter of the pores is uniform. Figure 2c shows the cross-section of a 400 nm empty AAO template, revealing that the pores are parallel and no interconnection is present among them. The surface of the AAO template after infiltration with PCL is shown in Figure 2d and 2e.

Figure 2f shows the cross-sectional morphology of a 400 nm AAO template infiltrated with PCL. It is clear that most of the nanopores are filled with polymer and there is no residual polymer on the template surface. A clean surface is essential for studying polymer crystallization within AAO nanopores.[41] For PBS, the top view of the 400 nm PBS-infiltrated AAO template is shown in Figure 2g. The side views of the 200 nm and 100 nm PBS-infiltrated AAO templates are shown in Figures 2h and 2i. Nanofibers are formed exhibiting a similar diameter with the nanopores of the respective AAO templates. These results indicate that the infiltrated PCL and PBS within AAO nanopores are in an ideal two-dimensional confinement environment.

3.2. Crystallization and Melting Behavior.

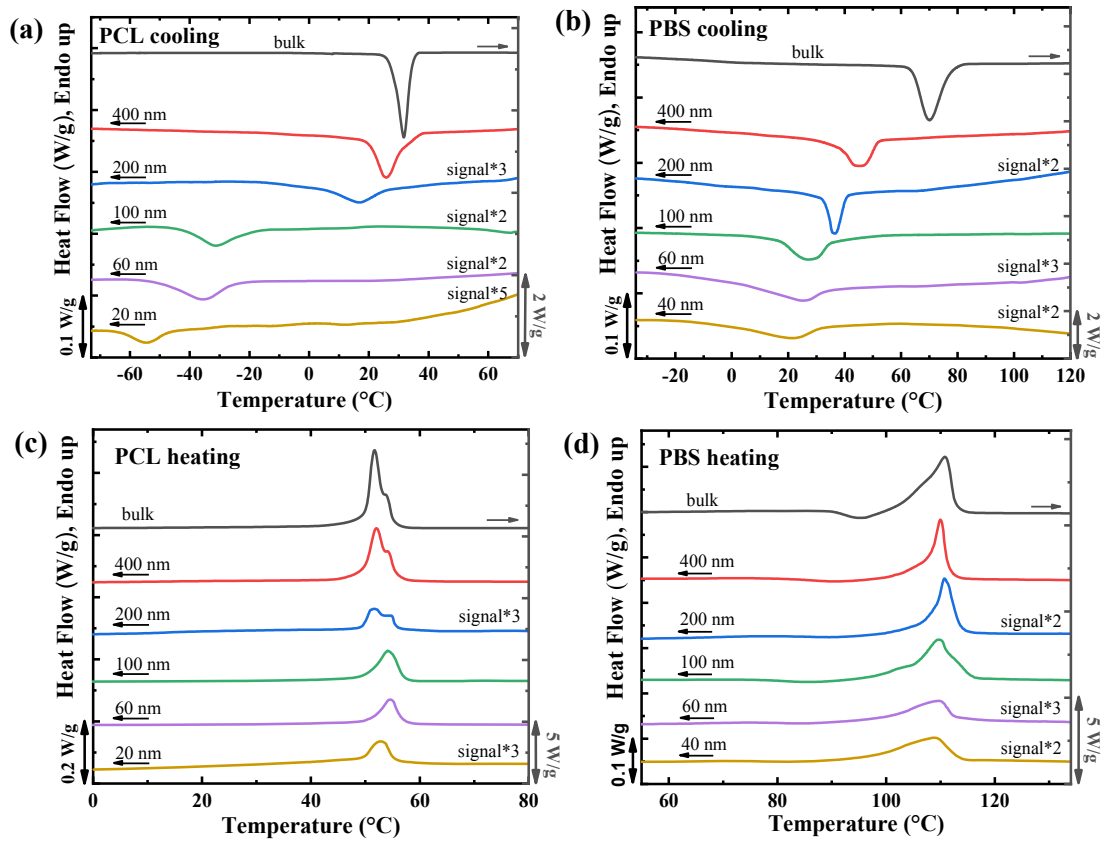

Figure 3. DSC cooling (a, b) and subsequent heating scans (c, d) of infiltrated PCL and PBS in AAO nanopores. Both the cooling and heating rates are 20 ºC/min.

Figure 3 shows the DSC cooling/heating scans of bulk and infiltrated PCL and PBS within AAO nanopores. The peak crystallization temperature (T_c) of bulk PCL is 32 ºC. Within 400, 200, 100, 60, and 20 nm AAO nanopores, the T_c of PCL decreases to 26, 17, -31 -36, and -54 ºC, respectively (see Figure 2a). For PBS, as shown in Figure 3b, the bulk PBS crystallizes at 70 ºC. Confined in AAO nanopores, the T_c decreases to 45, 36, 27, 26, and 21 ºC as the diameter of nanopores decreases from 400 nm to 40 nm. Figure 3c and 3d show the DSC heating traces of bulk and infiltrated PCL and PBS. Although the melting peak shape changes with the size of the pores, the melting temperatures (T_m) of all the PCL and PBS samples under different environments are roughly the same.

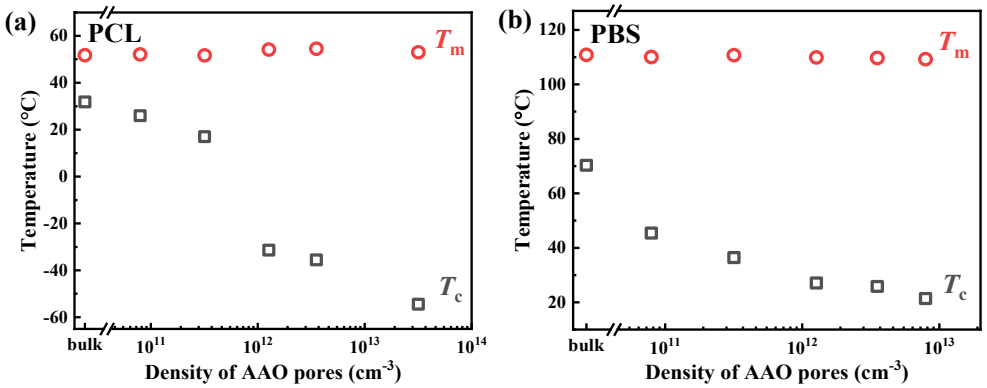

Figure 4. T_m and T_c of infiltrated PCL (a) and PBS (b) within AAO as a function of pore density. The density of nanopores was calculated according to their volume assuming that they are fully filled with polymer.

Figure 4 shows the T_m and T_c of infiltrated PCL and PBS in AAO templates (the exact values are summarized in Table 1) as a function of nanopore density. As the density of nanopores increases, the number of microdomains becomes much higher than that of the heterogeneous nuclei originally present in the bulk sample. The trend of PCL is similar to our previous report.[41]

The lowest T_c for infiltrated PCL in AAO nanopores is -54.4 ºC in this work, a value that is very close to the glass transition temperature (T_g) of PCL (-60 ºC[42]). The nucleation mechanism of infiltrated PCL that crystallizes at such a low temperature should be assigned to homogeneous nucleation because it occurs just above T_g. The abrupt decrease of T_c in nanopores smaller than 100 nm indicates a transition from heterogeneous to homogeneous nucleation.

For PBS, a drastic decrease of T_c of about 25 ºC can be seen in the 400 nm nanopores, and T_c further decreases as pore size decreases. In the smallest nanopores with a diameter of 40 nm in this work, T_c is about 21 ºC. Safari et al.[43] reported a T_c of 18 ºC for PBS confined in 35 nm AAO templates. Even in the smallest nanopores, the T_c is still ~ 50 ºC higher than the T_g of PBS (-30 ºC[43]). Therefore, the crystallization of infiltrated PBS in small nanopores most probably occurs by surface nucleation at the AAO pore walls.

Table 1. Crystallization and Melting Temperatures of Bulk and Infiltrated PCL and PBS.

sample	bulk	400 nm	200 nm	100 nm	60 nm	40 nm	20 nm
$T_{c,\,PCL}$ (°C)	31.9	25.9	17.0	-31.4	-35.6	-	-54.4
$T_{m,\,PCL}$ (°C)	51.8	52.1	51.7	54.2	54.5	-	53.0
$T_{c,\,PBS}$ (°C)	70.3	45.4	36.4	27.1	25.8	21.4	-
$T_{m,\,PBS}$ (°C)	110.8	110.1	110.7	109.9	109.7	109.3	-

3.3. Self-Nucleation Behavior of Bulk PCL and PBS.

Figure 5a shows DSC cooling curves of PCL after the isothermal step at the indicated T_s. The subsequent heating curves are shown in Figure 5b. The standard heating curve together with the crystallization temperatures is plotted in Figure 5c, with the three characteristic domains labeled[3, 4]. Classical self-nucleation features are displayed, similar to the results reported previously.[14, 15] The different self-nucleation *Domains* have been indicated by different colors for the DSC cooling and heating traces in Figure 5a and 5b (*Domain I* in red, *Domain II* in blue, and *Domain III* in green), as previously suggested in references.[3, 4]

At T_s > 64 °C, the material is molten into a homogeneous melt, the T_c is invariant for these T_s and the melting traces are unchanged in the subsequent heating process. Those T_s values are in

Domain I, at which the nuclei inducing crystallization are the high-temperature resistant heterogeneities.

When T_s is between 64 °C and 55 °C, PCL experiences exclusive self-nucleation, where T_c increases with decreasing T_s, as shown in Figure 5a. Meanwhile, the melting peaks in Figure 5b do not show any observable change. This is the classical *Domain II*. The width of *Domain II* is 9 °C (55 °C < T_s ≤ 64°C), which is similar to the previous reports.[14, 15] The *Domain IIa* (59 °C < T_s ≤ 64 °C) and *IIb* (55 °C < T_s ≤ 59 °C) can be discriminated with the help of the standard DSC heating curve shown in Figure 5c. In *Domain IIa*, the DSC trace has reached the baseline, indicating that all crystals are molten, hence the self-nucleation observed is due to melt memory effects[3, 4]. In *Domain IIb*, crystal fragments are present in the sample, as indicated by DSC, hence the self-nucleation is due to self-seeding from crystal fragments that are not annealed within this temperature *Domain*[2-4].

The sample is only partially molten when T_s is lower than 55 °C, and the unmelted crystals thicken (i.e., experience annealing) during the 5 min isothermal time at T_s. The T_c increases because of self-seeding, and an additional melting peak appears in the heating curves because of the annealing of unmolten crystals. Therefore, the sample is in *Domain III* (self-nucleation and annealing domain).

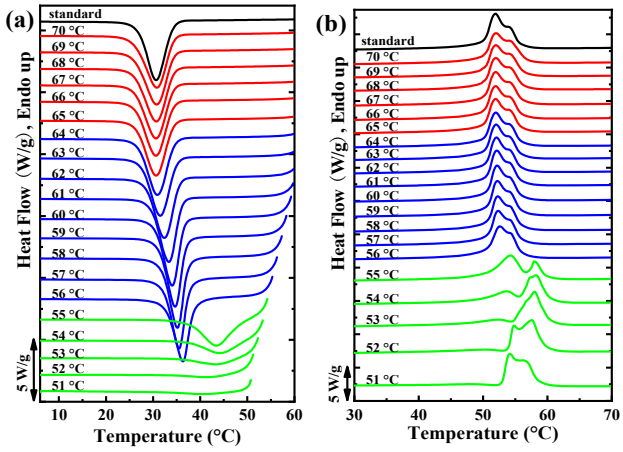

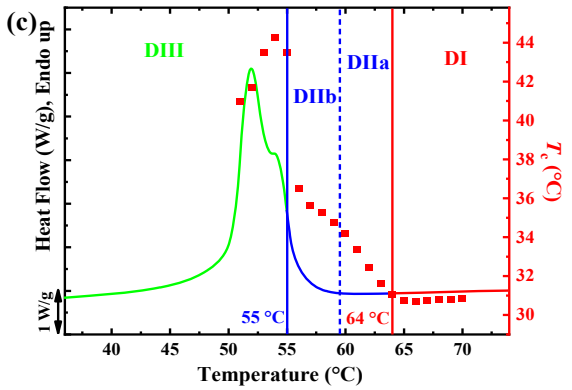

Figure 5. (a) DSC cooling scans for PCL after 5 min at the indicated T_s; (b) Subsequent heating scans; (c) Representation of the self-nucleation domains for PCL superimposed on the standard DSC heating curve. Red squares represent the T_c (right-hand side y-axis) as a function of T_s values (x-axis).

Figure 6 shows the SN experimental data of bulk PBS. Similar to PCL, it also displays three self-nucleation domains. The temperature range of *Domain I* is T_s > 121 °C. When 112 °C < T_s ≤ 121 °C, the material experiences self-nucleation (*Domain II*). When T_s lower than 112 °C, the melt traces start showing an annealing peak (*Domain III*). Within *Domain II, Domain IIa* is at 117 °C < T_s ≤ 121 °C and *IIb* is at 112 °C < T_s ≤ 117 °C. The width of *Domain II* is 9 °C for PBS, which can be seen directly from Figure 6c. The width of *Domain II* of PBS reported in ref.[44] is larger (18 °C). This might be attributed to the different molecular weights of the samples.

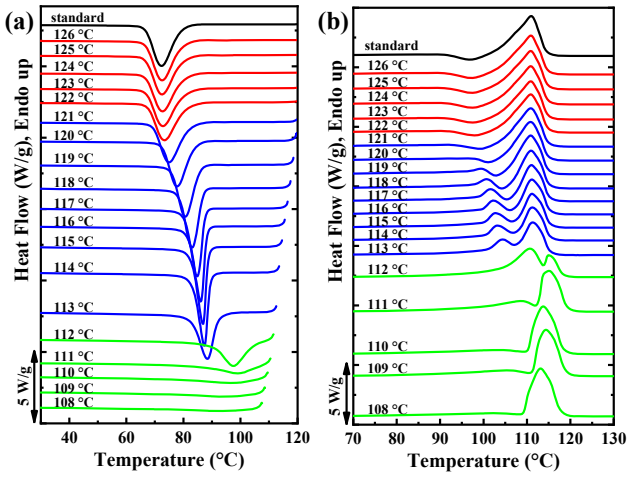

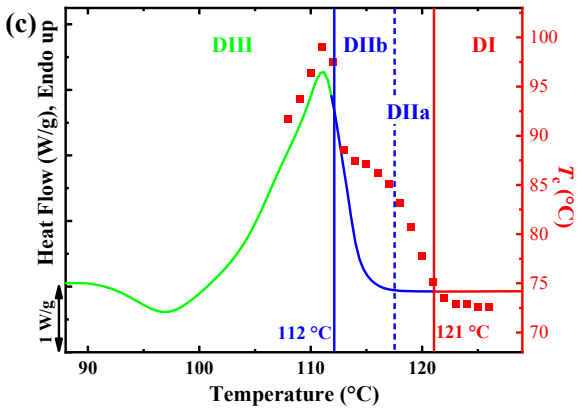

Figure 6. (a) DSC cooling scans for PBS after 5 min at the indicated T_s; (b) Subsequent heating scans after the corresponding cooling runs in (a); (c) Representation of the self-nucleation Domains for PBS superimposed on the standard DSC heating curve. Red squares represent the T_c (right-hand side y-axis) as a function of T_s values (x-axis).

3.4. Self-Nucleation Behavior of Infiltrated PCL in AAO Templates.

To quantitatively investigate the effect of confining size on the self-nucleation behavior, SN experiments were carried out for infiltrated PCL and PBS in AAO nanopores with a diameter ranging from 20 to 400 nm. The thermal protocol is the same as that applied to the bulk polymers.

A typical example of the SN of the infiltrated PCL within a 100 nm AAO template is shown in Figure 7. The transition temperature of *Domain I* to *II* is T_s = 56 ºC. At T_s = 56 ºC, another exothermic peak appears at ~ 13 ºC. This peak moves to a higher temperature and exhibits higher enthalpy when T_s decreases to 55 ºC. Meanwhile, the low-temperature peak remains at the same temperatures but becomes smaller. An annealing peak appears in the DSC heating curve when T_s = 54 ºC. Therefore, the range of *Domain II* for this sample is 54 ºC < T_s ≤ 56 ºC (and it corresponds to *Domain IIb*, see below and Figure 7c). The width of *Domain II* is 2 ºC, narrower than the bulk sample (9 ºC). Interestingly, by comparing the T_c values with the standard DSC heating curve (Figure 7c), it is clear that *Domain IIa* vanishes. The enthalpy (ΔH_c) of the lowest crystallization peak shows a sudden decrease in *Domain II*, as shown in Figure 7c.

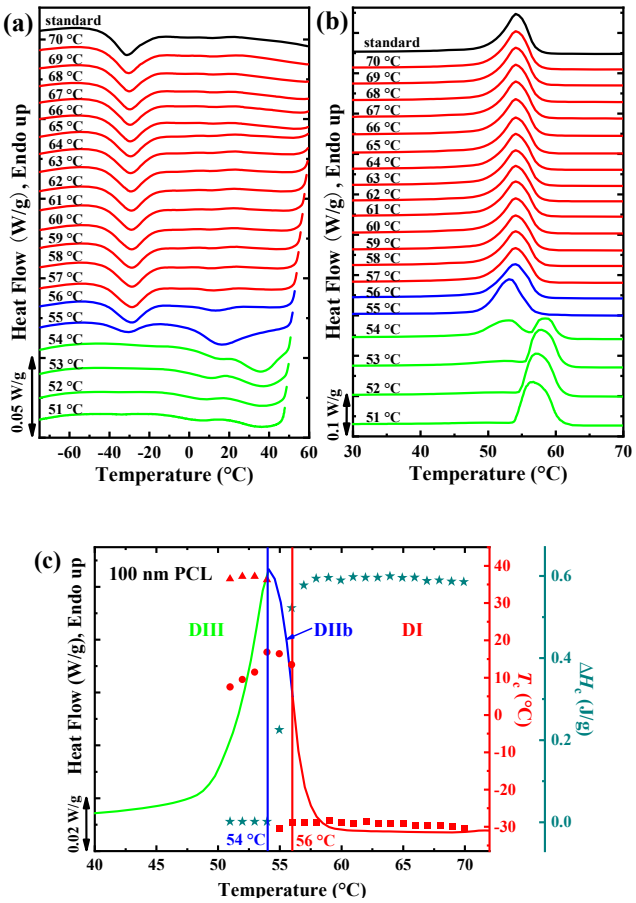

Figure 7. (a) DSC cooling scans for PCL confined within 100 nm AAO nanopores after staying for 5 min at the indicated T_s values; (b) Subsequent heating scans after the corresponding cooling runs in (a); (c) Representation of the self-nucleation domains for PCL superimposed on the standard DSC melting trace. Red points represent peak crystallization temperatures. The crystallization enthalpy (ΔH_c) of the crystallization peak at -30 ºC is also plotted (dark cyan star).

The SN results of bulk and confined samples are summarized in Figure 8 (DSC scans are shown in Figures S1 to S5 in the supporting information). The transition temperatures of different *Domains* are summarized in Table 2 and Figure 10. As the diameter of AAO templates decreased, the width of *Domain II* of PCL decreased from 9 ºC in bulk to 6 ºC in 400 nm AAO, and further to 3 °C, 2 °C, 1 ºC in 200, 100, 60 nm AAO, respectively. *Domain II* vanishes completely when the diameter of AAO is 20 nm. Another interesting observation is that the width of *Domain IIa* changes first. For example, the "shrinkage" of *Domain II* for the 400 nm PCL solely comes from *Domain IIa*. Furthermore, *Domain IIa* vanishes for the 200 nm sample. The direct transition from *Domain I* to *Domain III* has been reported in block copolymers.[19, 22] To the best of our knowledge,

we have shown here for the first time a continuous change of the width of *Domain II*, caused by confinement.

Table 2. Summary of the transition temperature of different domains of PCL and PBS.

sample		$T_{s,\ DI\ to\ DII}$ (ºC)	$T_{s,\ DII\ to\ DIII}$ (ºC)	$T_{s,\ DI\ to\ DIII}$ (ºC)
PCL	bulk	64	55	-
	400 nm	61	55	-
	200 nm	58	55	-
	100 nm	56	54	-
	60 nm	55	54	-
	20 nm	-	-	52
PBS	bulk	121	112	-
	400 nm	120	111	-
	200 nm	121	112	-
	100 nm	118	112	-
	60 nm	112	111	-
	40 nm	-	-	112

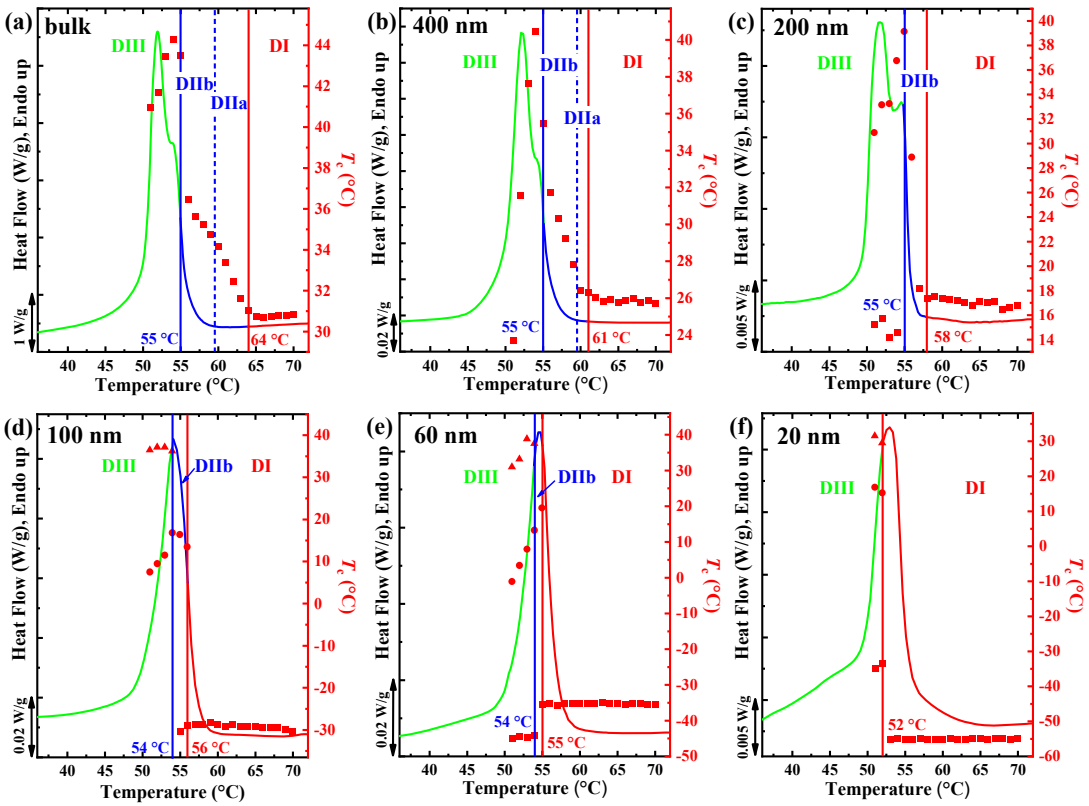

Figure 8. Representation of the self-nucleation *Domains* for bulk PCL (a), and infiltrated PCL

within 400 nm (b), 200 nm (c), 100 nm (d), 60 nm (e), and 20 nm (f) AAO templates superimposed on the standard DSC melting traces. Red points represent peak crystallization temperatures (right-hand side y-axis) as a function of T_s values (x-axis).

3.5. Self-Nucleation Behavior of Infiltrated PBS in AAO Templates.

SN experiments were carried out for infiltrated PBS using the same thermal protocol as for the bulk sample. The results are summarized in Figure 9 and the DSC curves are shown in Figure S6 to S10 in the supporting information. Different from PCL, the width of the *Domain II* of the PBS in 400 nm and 200 nm AAO is the same as that of bulk PBS. The width of *Domain II* decreases upon further confinement. The width of *Domain II* decreases to 6 ºC and 2 ºC for the infiltrated PBS within 100 nm and 60 nm AAO. Eventually, *Domain II* completely vanishes for the 40 nm sample. The transition temperatures of different domains of PBS are summarized in Table 2 and plotted in Figure 10.

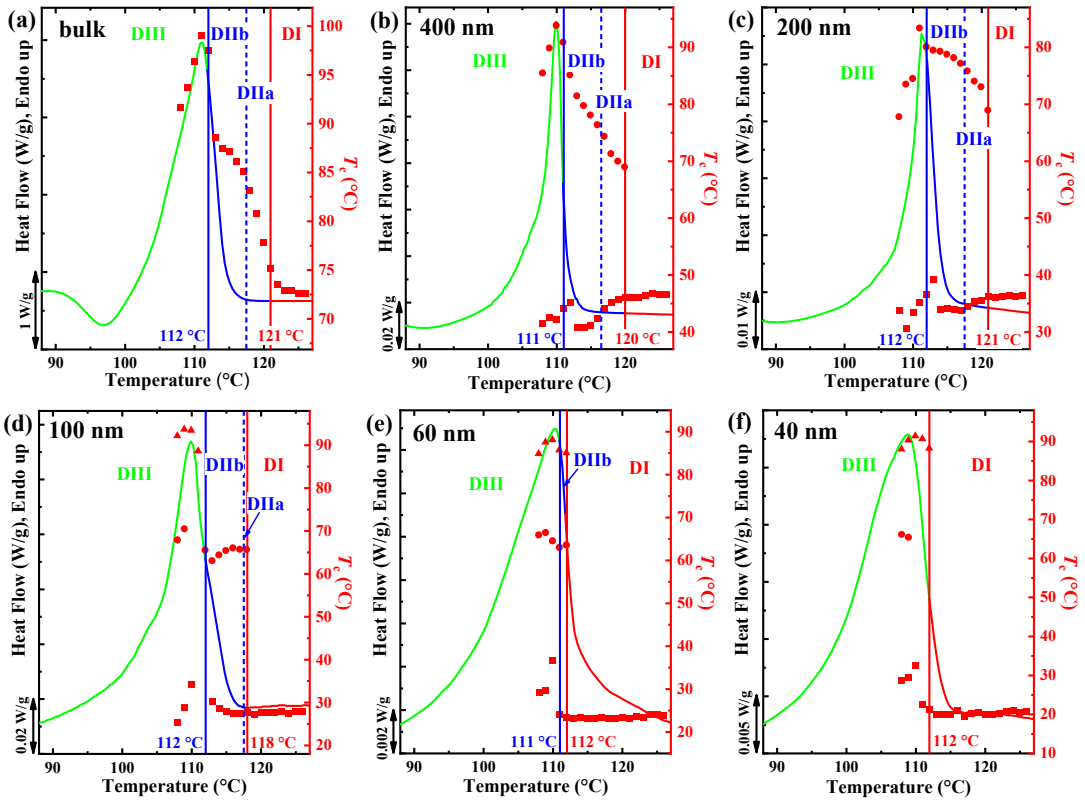

Figure 9. Representation of the self-nucleation Domains for bulk PBS (a), and infiltrated PBS in 400 nm (b), 200 nm (c), 100 nm (d), 60 nm (e), and 40 nm (f) AAO templates superimposed on the standard DSC melting trace. Red points represent peak crystallization temperatures (right-hand

side y-axis) as a function of T_s values (x-axis).

3.6. Confinement Effects on SN.

The change of the width of *Domain IIa/IIb* with the diameter/density of AAO nanopores is summarized in Figure 10. The estimated values of the number density of AAO nanopores with different diameters are listed in Table S1. We can see clearly that the upper limit of *Domain II* decreases with decreasing AAO nanopore diameter. *Domain IIa* vanishes first then *Domain IIb* vanishes eventually as nanopore diameters are further decreased.

The first conclusion is that the self-nucleation effect in confined systems is determined by the relative density of the self-nuclei and microdomains. In confined systems, the self-nuclei will be active to trigger crystallization only when its number exceeds the number of microdomains. The absence of *Domain II* under confinement has been observed in block copolymers.[45, 46] In triblock copolymers, PS-*b*-PB-*b*-PCL and PS-*b*-PEO-*b*-PCL, PCL blocks are confined within cylinders or spheres of densities approaching $10^{16}/cm^3$, much higher than that of the AAO templates. An advantage of the AAO system is that the scale of the microdomain density covers a broad range, thereby allowing the observation of the narrowing and vanishing process of *Domain II*.

In another aspect, the results provide an estimation of the densities of self-nuclei. For example, the PCL 400 nm sample is in *Domain IIb* at T_s = 58 ºC but the PCL 200 nm sample is in *Domain I* at the same temperature. Therefore, we can conclude that the self-nuclei density of PCL at T_s = 58 ºC is between 8×10^{10} and 3.2×10^{11} nuclei/cm^3. Based on this analysis, it may be of interest to compare the difference between the two polymers. The change of *Domain II* is very sharp in PBS. The densities of self-nuclei are all above the nanopore density of 200 nm AAO (3.2×10^{11} cm^{-3}) in the T_s range of 113 ~ 121 ºC. The sharp decrease of the width of *Domain II* in PBS indicates that the density of self-nuclei is as high as a value between 1.3×10^{12} (100 nm) and 3.5×10^{12} cm^{-3} (60 nm). On the other hand, the density of self-nuclei in PCL is lower and the change of *Domain II* is a gradual process. It is possible to estimate the value of self-nuclei for PCL in the temperature range of 55 ~ 65 ºC.

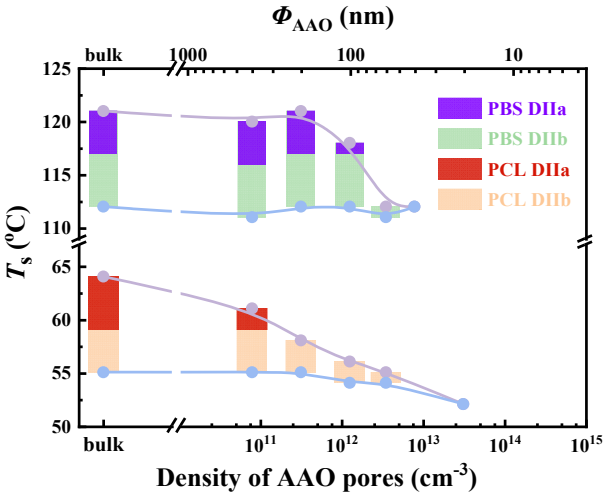

Figure 10. The transition temperatures of *Domain IIa/IIb* as a function of the density of AAO pores and pore diameter (Φ_{AAO}).

Another interesting effect of confinement is the fractionated crystallization behavior of the self-nucleated sample, i.e., multiple crystallization peaks. Fractionated crystallization behavior is frequently seen in immiscible polymer blends where crystalline components are in isolated domains.[47] The reason for the phenomenon is the existence of nucleating heterogeneities with different activities that are physically divided into different domains. For a full understanding of fractionated crystallization in different systems, the reader is referred to the recent reviews[48, 49].

The fractionation behavior differs in *Domain II* and *Domain III*. Let's first focus on *Domain II*. Two crystallization peaks are observed in infiltrated PCL within 100 nm and 60 nm AAO and all the infiltrated PBS samples except the 40 nm one. The results can be explained by the fact that the microdomains can be divided into the ones that contain self-nuclei and the ones that do not. The former can crystallize at higher temperatures than the latter because they are physically separated.

The fractionated crystallization behavior in *Domain III* is more complicated. With decreasing the pore size of AAO, the number of crystallization peaks changes from one (bulk) to two (200 and 100 nm PCL; 400 and 200 nm PBS) to three (below 60 nm for PCL; below 100 nm for PBS). The lowest peak can be originated from those impurity-free nanopores that are not affected by self-nucleation at all. The highest peak is most probably due to the residual crystals that can be

annealed which will grow immediately during cooling. The intermediate crystallization peak should be the domains that contain self-nuclei but do not contain crystals that can be annealed.

4. CONCLUSIONS

In this work, we studied the effect of confinement on the self-nucleation effect of semi-crystalline PCL and PBS. The density of AAO nanopores covers a range of 10^{11}~10^{13} cm^{-3}, a suitable scale for studying the self-nucleation effect. In both of the two polymers, the *Domain IIa*, or *melt memory region*, vanished first, and the *Domain IIb* (self-seeding region), disappeared subsequently, indicating a complete suppression of the *self-nucleation Domain* (i.e., *Domain II*). The results can be interpreted by the relative magnitudes of the density of self-nuclei and density of microdomains. In PCL, the change of the width of *Domain II* is more "continuous" as compared to PBS where an abrupt decrease of *Domain II* at the pore density of 10^{12} cm^{-3} occurs. The AAO system provided a new method to estimate the density of self-nuclei in different polymers.

ASSOCIATED CONTENT

Supporting Information

DSC curves of SN experiments of confined PCL and PBS (Figures S1-10), and the number density of AAO nanopores with different diameters (Tables S1) (PDF)

ACKNOWLEDGEMENTS

This work is supported by the National Natural Science Foundation of China (21873109, 51820105005, and 21922308) and the National Key R&D Program of China (2017YFE0117800). We would also like to acknowledge the financial support from the BIODEST project; this project has received funding from the European Union's Horizon 2020 research and innovation programme under the Marie Skłodowska-Curie grant agreement No 778092. G.L. is grateful to the Youth Innovation Promotion Association of the Chinese Academy of Sciences (Y201908).

REFERENCES

1. Blundell, D. J.; Keller, A.; Kovacs, A. J. A new self-nucleation phenomenon and its application to

the growing of polymer crystals from solution. *J. Polym. Sci. Part B: Polym. Lett.* **1966,** 4 (7), 481-486 DOI: 10.1002/pol.1966.110040709.

2. Fillon, B.; Wittmann, J. C.; Lotz, B.; Thierry, A. Self-nucleation and recrystallization of isotactic polypropylene (α phase) investigated by differential scanning calorimetry. *J. Polym. Sci. Part B: Polym. Phys.* **1993,** 31 (10), 1383-1393 DOI: 10.1002/polb.1993.090311013.

3. Sangroniz, L.; Cavallo, D.; Müller, A. J. Self-Nucleation Effects on Polymer Crystallization. *Macromolecules* **2020,** 53 (12), 4581-4604 DOI: 10.1021/acs.macromol.0c00223.

4. Michell, R. M.; Mugica, A.; Zubitur, M.; Müller, A. J., Self-Nucleation of Crystalline Phases Within Homopolymers, Polymer Blends, Copolymers, and Nanocomposites. In *Polymer Crystallization I: From Chain Microstructure to Processing*, Auriemma, F., Alfonso, G. C., de Rosa, C., Eds. Springer International Publishing: Cham, 2017; pp 215-256.

5. Lorenzo, A. T.; Arnal, M. L.; Sánchez, J. J.; Müller, A. J. Effect of annealing time on the self-nucleation behavior of semicrystalline polymers. *J. Polym. Sci. Part B: Polym. Phys.* **2006,** 44 (12), 1738-1750 DOI: 10.1002/polb.20832.

6. Sangroniz, L.; Ocando, C.; Cavallo, D.; Müller, A. J. Melt Memory Effects in Poly(butylene succinate) Studied by Differential Fast Scanning Calorimetry. *Polymers* **2020,** 12 (12), 2796 DOI: 10.3390/polym12122796.

7. Xu, J.; Ma, Y.; Hu, W.; Rehahn, M.; Reiter, G. Cloning polymer single crystals through self-seeding. *Nat. Mater.* **2009,** 8, 348 DOI: 10.1038/nmat2405.

8. Luo, C.; Sommer, J.-U. Frozen Topology: Entanglements Control Nucleation and Crystallization in Polymers. *Phys. Rev. Lett.* **2014,** 112 (19), 195702. DOI: https://doi.org/10.1103/PhysRevLett.112.195702.

9. Muthukumar, M. Communication: Theory of melt-memory in polymer crystallization. *J. Chem. Phys.* **2016,** 145 (3), 031105 DOI: 10.1063/1.4959583.

10. Reid, B. O.; Vadlamudi, M.; Mamun, A.; Janani, H.; Gao, H.; Hu, W.; Alamo, R. G. Strong Memory Effect of Crystallization above the Equilibrium Melting Point of Random Copolymers. *Macromolecules* **2013,** 46 (16), 6485-6497 DOI: 10.1021/ma400839d.

11. Cavallo, D.; Gardella, L.; Portale, G.; Müller, A. J.; Alfonso, G. C. Self-nucleation of isotactic poly(1-butene) in the trigonal modification. *Polymer* **2014,** 55 (1), 137-142 DOI: https://doi.org/10.1016/j.polymer.2013.11.030.

12. Maus, A.; Hempel, E.; Thurn-Albrecht, T.; Saalwächter, K. Memory effect in isothermal crystallization of syndiotactic polypropylene --Role of melt structure and dynamics? *Eur. Phys. J. E* **2007,** 23 (1), 91 DOI: 10.1140/epje/i2007-10183-6.

13. Sangroniz, L.; Cavallo, D.; Santamaria, A.; Müller, A. J.; Alamo, R. G. Thermorheologically Complex Self-Seeded Melts of Propylene–Ethylene Copolymers. *Macromolecules* **2017,** 50 (2), 642-651 DOI: 10.1021/acs.macromol.6b02392.

14. Sangroniz, L.; Alamo, R. G.; Cavallo, D.; Santamaría, A.; Müller, A. J.; Alegría, A. Differences between Isotropic and Self-Nucleated PCL Melts Detected by Dielectric Experiments. *Macromolecules* **2018,** 51 (10), 3663-3671 DOI: 10.1021/acs.macromol.8b00708.

15. Sangroniz, L.; Barbieri, F.; Cavallo, D.; Santamaria, A.; Alamo, R. G.; Müller, A. J. Rheology of self-nucleated poly(ε-caprolactone) melts. *Eur. Polym. J.* **2018,** 99, 495-503 DOI: https://doi.org/10.1016/j.eurpolymj.2018.01.009.

16. Liu, X.; Wang, Y.; Wang, Z.; Cavallo, D.; Müller, A. J.; Zhu, P.; Zhao, Y.; Dong, X.; Wang, D. The origin of memory effects in the crystallization of polyamides: Role of hydrogen bonding. *Polymer* **2020,**

188, 122117 DOI: https://doi.org/10.1016/j.polymer.2019.122117.

17. Sangroniz, L.; Sangroniz, A.; Meabe, L.; Basterretxea, A.; Sardon, H.; Cavallo, D.; Müller, A. J. Chemical Structure Drives Memory Effects in the Crystallization of Homopolymers. *Macromolecules* **2020,** 53 (12), 4874-4881 DOI: 10.1021/acs.macromol.0c00751.

18. Gao, H.; Vadlamudi, M.; Alamo, R. G.; Hu, W. Monte Carlo Simulations of Strong Memory Effect of Crystallization in Random Copolymers. *Macromolecules* **2013,** 46 (16), 6498-6506 DOI: 10.1021/ma400842h.

19. Schmalz, H.; Müller, A. J.; Abetz, V. Crystallization in ABC Triblock Copolymers with Two Different Crystalline End Blocks: Influence of Confinement on Self-Nucleation Behavior. *Macromol. Chem. Phys.* **2003,** 204 (1), 111-124 DOI: https://doi.org/10.1002/macp.200290063.

20. Müller, A. J.; Albuerne, J.; Marquez, L.; Raquez, J.-M.; Degée, P.; Dubois, P.; Hobbs, J.; Hamley, I. W. Self-nucleation and crystallization kinetics of double crystalline poly(p-dioxanone)-b-poly(ε-caprolactone) diblock copolymers. *Faraday Discussions* **2005,** 128 (0), 231-252 DOI: 10.1039/B403085K.

21. Arnal, M. L.; López-Carrasquero, F.; Laredo, E.; Müller, A. J. Coincident or sequential crystallization of PCL and PEO blocks within polystyrene-b-poly(ethylene oxide)-b-poly(ε-caprolactone) linear triblock copolymers. *Eur. Polym. J.* **2004,** 40 (7), 1461-1476 DOI: https://doi.org/10.1016/j.eurpolymj.2004.02.023.

22. Balsamo, V.; Paolini, Y.; Ronca, G.; Müller, A. J. Crystallization of the polyethylene block in polystyrene-b-polyethylene-b-polycaprolactone triblock copolymers, 1. Self-nucleation behavior. *Macromol. Chem. Phys.* **2000,** 201 (18), 2711-2720 DOI: https://doi.org/10.1002/1521-3935(20001201)201:18<2711::AID-MACP2711>3.0.CO;2-6.

23. Colonna, S.; Perez-Camargo, R. A.; Chen, H. M.; Liu, G. M.; Wang, D. J.; Muller, A. J.; Saracco, G.; Fina, A. Supernucleation and Orientation of Poly(butylene terephthalate) Crystals in Nanocomposites Containing Highly Reduced Graphene Oxide. *Macromolecules* **2017,** 50 (23), 9380-9393 DOI: 10.1021/acs.macromol.7b01865.

24. Wen, X.; Su, Y.; Shui, Y.; Zhao, W.; Müller, A. J.; Wang, D. Correlation between Grafting Density and Confined Crystallization Behavior of Poly(ethylene glycol) Grafted to Silica. *Macromolecules* **2019,** 52 (4), 1505-1516 DOI: 10.1021/acs.macromol.8b02007.

25. Wu, H.; Higaki, Y.; Takahara, A. Molecular self-assembly of one-dimensional polymer nanostructures in nanopores of anodic alumina oxide templates. *Prog. Polym. Sci.* **2018,** 77, 95-117 DOI: https://doi.org/10.1016/j.progpolymsci.2017.10.004.

26. Samanta, P.; Liu, C.-L.; Nandan, B.; Chen, H.-L., Chapter 13 - Crystallization of Polymers in Confined Space A2 - Thomas, Sabu. In *Crystallization in Multiphase Polymer Systems*, P, M. A., Gowd, E. B., Kalarikkal, N., Eds. Elsevier: 2018; pp 367-431.

27. Michell, R. M.; Müller, A. J. Confined crystallization of polymeric materials. *Progress in Polymer Science* **2016,** 54, 183-213 DOI: http://dx.doi.org/10.1016/j.progpolymsci.2015.10.007.

28. Liu, G.; Shi, G.; Wang, D. Research Progress on Polymer Crystallization Confined within Nano-porous AAO Templates. *Acta Polym. Sin.* **2020,** 51 (5), 501-516 DOI: 10.11777/j.issn1000-3304.2020.20003.

29. Duran, H.; Steinhart, M.; Butt, H.-J.; Floudas, G. From Heterogeneous to Homogeneous Nucleation of Isotactic Poly(propylene) Confined to Nanoporous Alumina. *Nano Lett.* **2011,** 11 (4), 1671-1675 DOI: 10.1021/nl200153c.

30. Michell, R. M.; Lorenzo, A. T.; Müller, A. J.; Lin, M.-C.; Chen, H.-L.; Blaszczyk-Lezak, I.;

Martín, J.; Mijangos, C. The Crystallization of Confined Polymers and Block Copolymers Infiltrated Within Alumina Nanotube Templates. *Macromolecules* **2012,** (45), 1517-1528 DOI: 10.1021/ma202327f.

31. Steinhart, M.; Goring, P.; Dernaika, H.; Prabhukaran, M.; Gosele, U.; Hempel, E.; Thurn-Albrecht, T. Coherent kinetic control over crystal orientation in macroscopic ensembles of polymer nanorods and nanotubes. *Phys. Rev. Lett.* **2006,** 97 (2), 027801 DOI: 10.1103/PhysRevLett.97.027801.

32. Su, C.; Shi, G.; Li, X.; Zhang, X.; Müller, A. J.; Wang, D.; Liu, G. Uniaxial and Mixed Orientations of Poly(ethylene oxide) in Nanoporous Alumina Studied by X-ray Pole Figure Analysis. *Macromolecules* **2018,** 51 (23), 9484-9493 DOI: 10.1021/acs.macromol.8b01801.

33. Su, C.; Shi, G.; Wang, D.; Liu, G. A Model for the Crystal Orientation of Polymers Confined in 1D Nanocylinders. *Acta Polymerica Sinica* **2019**, DOI: 10.11777/j.issn1000-3304.2018.18218.

34. Liu, C.-L.; Chen, H.-L. Variable Crystal Orientation of Poly(ethylene oxide) Confined within the Tubular Space Templated by Anodic Aluminum Oxide Nanochannels. *Macromolecules* **2017,** 50 (2), 631-641 DOI: 10.1021/acs.macromol.6b02347.

35. Shin, K.; Woo, E.; Jeong, Y. G.; Kim, C.; Huh, J.; Kim, K.-W. Crystalline Structures, Melting, and Crystallization of Linear Polyethylene in Cylindrical Nanopores. *Macromolecules* **2007,** 40 (18), 6617-6623 DOI: 10.1021/ma070994e.

36. Michell, R. M.; Blaszczyk-Lezak, I.; Mijangos, C.; Müller, A. J. Confinement effects on polymer crystallization: From droplets to alumina nanopores. *Polymer* **2013,** 54 (16), 4059-4077 DOI: https://doi.org/10.1016/j.polymer.2013.05.029.

37. Su, C.; Chen, Y.; Shi, G.; Li, T.; Liu, G.; Müller, A. J.; Wang, D. Crystallization Kinetics of Poly(ethylene oxide) under Confinement in Nanoporous Alumina Studied by in Situ X-ray Scattering and Simulation. *Langmuir* **2019,** 35 (36), 11799-11808 DOI: 10.1021/acs.langmuir.9b01968.

38. Li, L.; Liu, J.; Qin, L.; Zhang, C.; Sha, Y.; Jiang, J.; Wang, X.; Chen, W.; Xue, G.; Zhou, D. Crystallization kinetics of syndiotactic polypropylene confined in nanoporous alumina. *Polymer* **2017,** 110 (Supplement C), 273-283 DOI: https://doi.org/10.1016/j.polymer.2016.12.081.

39. Mi, C.; Zhou, J.; Ren, Z.; Li, H.; Sun, X.; Yan, S. The phase transition behavior of poly(butylene adipate) in the nanoporous anodic alumina oxide. *Polym. Chem.* **2016,** 7 (2), 410-417 DOI: 10.1039/C5PY01532D.

40. Shi, G.; Wang, Z.; Wang, M.; Liu, G.; Cavallo, D.; Müller, A. J.; Wang, D. Crystallization, Orientation, and Solid–Solid Crystal Transition of Polybutene-1 Confined within Nanoporous Alumina. *Macromolecules* **2020,** 53 (15), 6510-6518 DOI: 10.1021/acs.macromol.0c01384.

41. Shi, G.; Liu, G.; Su, C.; Chen, H.; Chen, Y.; Su, Y.; Müller, A. J.; Wang, D. Reexamining the Crystallization of Poly(ε-caprolactone) and Isotactic Polypropylene under Hard Confinement: Nucleation and Orientation. *Macromolecules* **2017,** 50 (22), 9015-9023 DOI: 10.1021/acs.macromol.7b02284.

42. Modjarrad, K.; Ebnesajjad, S., *Handbook of polymer applications in medicine and medical devices*. Elsevier: 2013.

43. Safari, M.; Maiz, J.; Shi, G.; Juanes, D.; Liu, G.; Wang, D.; Mijangos, C.; Alegría, Á.; Müller, A. J. How Confinement Affects the Nucleation, Crystallization, and Dielectric Relaxation of Poly(butylene succinate) and Poly(butylene adipate) Infiltrated within Nanoporous Alumina Templates. *Langmuir* **2019,** 35 (47), 15168-15179 DOI: 10.1021/acs.langmuir.9b02215.

44. Arandia, I.; Mugica, A.; Zubitur, M.; Arbe, A.; Liu, G.; Wang, D.; Mincheva, R.; Dubois, P.; Müller, A. J. How Composition Determines the Properties of Isodimorphic Poly(butylene

succinate-ran-butylene azelate) Random Biobased Copolymers: From Single to Double Crystalline Random Copolymers. *Macromolecules* **2015,** 48 (1), 43-57 DOI: 10.1021/ma5023567.

45. Müller, A. J.; Arnal, M. L.; López-Carrasquero, F. Nucleation and crystallization of PS-b-PEO-b-PCL triblock copolymers. *Macromol. Symp.* **2002,** 183 (1), 199-204 DOI: https://doi.org/10.1002/1521-3900(200207)183:1<199::AID-MASY199>3.0.CO;2-S.

46. Müller, A. J.; Balsamo, V.; Arnal, M. L.; Jakob, T.; Schmalz, H.; Abetz, V. Homogeneous Nucleation and Fractionated Crystallization in Block Copolymers. *Macromolecules* **2002,** 35 (8), 3048-3058 DOI: 10.1021/ma012026w.

47. Frensch, H.; Jungnickel, B. J. Some novel crystallization kinetic peculiarities in finely dispersing polymer blends. *Colloid Polym. Sci.* **1989,** 267 (1), 16-27 DOI: 10.1007/bf01410144.

48. Groeninckx, G.; Harrats, C.; Vanneste, M.; Everaert, V., Crystallization, Micro- and Nano-structure, and Melting Behavior of Polymer Blends. In *Polymer Blends Handbook*, Utracki, L. A., Wilkie, C. A., Eds. Springer Netherlands: Dordrecht, 2014; pp 291-446.

49. Sangroniz, L.; Wang, B.; Su, Y.; Liu, G.; Cavallo, D.; Wang, D.; Müller, A. J. Fractionated crystallization in semicrystalline polymers. *Prog. Polym. Sci.* **2021**, 101376 DOI: https://doi.org/10.1016/j.progpolymsci.2021.101376.